Electronic Supplementary Information

Supporting ultrathin fish-scale-like BiOBr nanosheets on $Bi_6Mo_2O_{15}$ sub-microwires for boosting photocatalytic performance

Gui Yang [a], Yujun Liang [a, *], Jian Yang [a], Kun Wang [a], Zikang Zeng [a] and Zhuoran Xiong [a]

[a] *Engineering Research Center of Nano-Geomaterials of Ministry of Education, Faculty of Materials Science and Chemistry, China University of Geosciences, Wuhan 430074, China*

[*]**Corresponding author:** Tel: +86 27 67884814; fax: +86 27 67883733.

E-mail address: yujunliang@sohu.com (Yujun Liang)

Experimental section

Preparation of photocatalysts

Two synthesis processes were used to synthesize the ($BiOBr/Bi_6Mo_2O_{15}$) heterojunctions.

(1) Molten salt-assisted synthesis process ($Bi_6Mo_2O_{15}$). $NaNO_3$ with the eutectic point of 308 °C was employed as the molten salt, and the mass ratio of molten salts to raw materials was 8:1. Typically, 1.21 g of $Bi(NO_3)_3 \cdot 5H_2O$ and 0.91 g $Na_2MoO_4 \cdot 2H_2O$ were fully ground for about 15 min. Subsequently, the mixture was further grinded with 0.8499 g $NaNO_3$ for more than 30 min to form a well-dispersed mixture. The mixed powders were heated at 500 °C for 10 h in air. Finally, the obtained samples were treated with the hot deionized water and ethanol to remove $NaNO_3$. Finally, the obtained samples were dried at 80 °C for 24 h

(2) Surface chemical etching process ($BiOBr/Bi_6Mo_2O_{15}$). The $BiOBr/Bi_6Mo_2O_{15}$ edge-on heterostructure was further fabricated by using a simple chemical etching strategy. Typically, 0.1 g of $Bi_6Mo_2O_{15} \cdot 5H_2O$ was dissolved in HNO_3 (30 mL, 0.5 mol L^{-1}), termed as solution A. 1.6 g of KBr were dissolved in 10 mL de-ionized water, termed as solution B. Subsequently, solution B was dropwise added into solution A. After vigorously stirring for 30 min, the resultant samples were rinsed using the deionized water and ethanol, and then dried at 80 °C for further use.

Characterization

Powder X-ray diffraction (XRD) data of the as-prepared samples were collected on an X-ray diffractometer (D8-FOCUS, Bruker, Germany) with Cu Kα radiation (λ = 1.5418 Å). The morphology and microstructure observation were examined by field emission scanning electron microscope (FE-SEM, SU8010, Hitachi, Japan) and transmission electron microscope (TEM, Tecnai G2 T20, FEI, America). Meanwhile, the energy-dispersive X-ray spectroscopy (EDS) spectra and elemental mapping images were collected in an EDAX Genesis, which was attached to the FE-SEM. X-ray photoelectron spectroscopy (XPS) measurement was performed on a Thermo Scientific Escalab 250X spectrometer equipped with an Al Kα X-ray source. UV-vis diffuse reflectance spectra (DRS) were tested on an UV-2550PC spectrophotometer (Shimadzu Corporation, Japan), using $BaSO_4$ as the reflectance standard. The photoluminescence (PL) spectra of photocatalysts were measured by a fluorescence spectrometer (Fluoromax-4P, Horiba Jobin Yvon, New Jersey, USA), which was equipped with a 150 W xenon lamp as the excitation source.

Photocatalytic measurements

The photocatalytic performances of all catalysts were measured by photodegradation of tetracycline (TC). The photocatalytic experiments were conducted in a multipath photochemical reaction system (PCX50B, Beijing Perfect Light Technology co., LTD). A 5 W white LED was used as a visible light source with the light intensity of 72.9 $mW \cdot cm^{-2}$ and thespectral range of LED light is displayed in Fig. S1. Typically,

20 mg samples were dispersed in 50 mL TC solution (10 mg/L) for photocatalytic activity tests. The residual concentration of TC was determined by UV-vis spectrophotometer at a maximum absorbance wavelength of 357 nm. In addition, the intermediates of residue TC were further analyzed on a HPLC-MS system (Agilent 1200 HPLC 6460A MS/MS, USA).

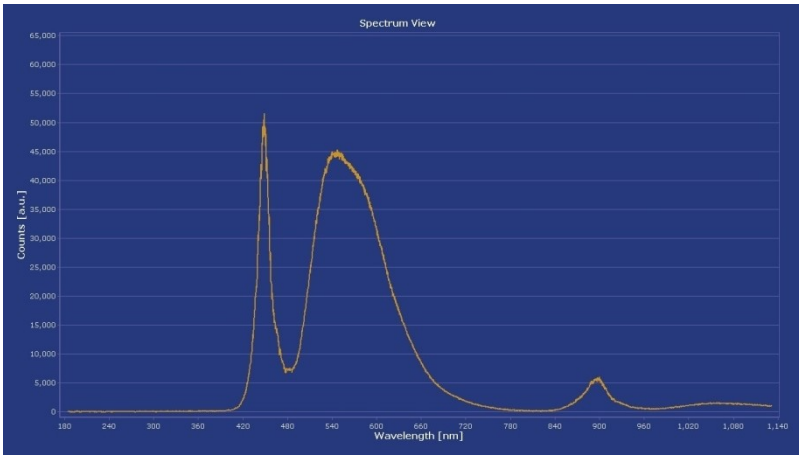

Fig. S1 The light emission spectrum of LED.

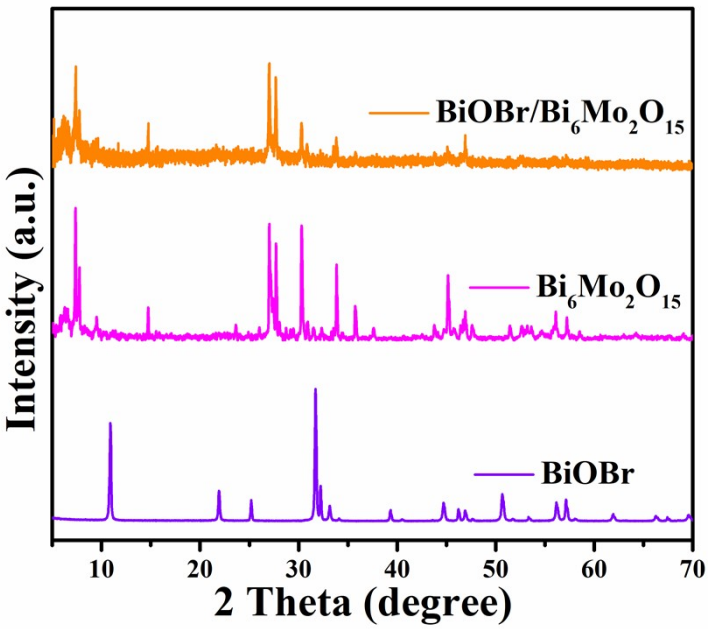

Fig. S2 The XRD patterns of as-obtained samples.

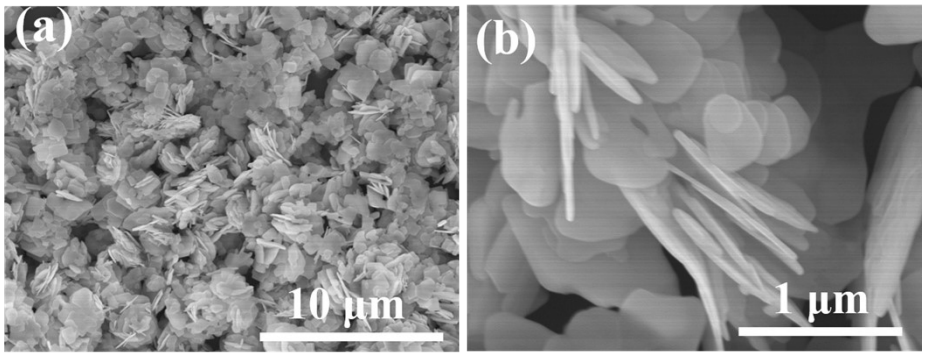

Fig. S3 (a) SEM images of pure BiOBr.

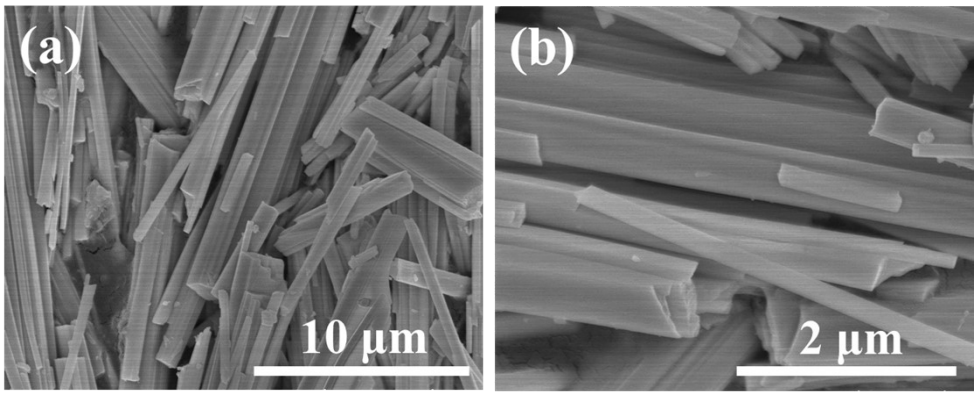

Fig. S4 The SEM images of $Bi_6Mo_2O_{15}$.

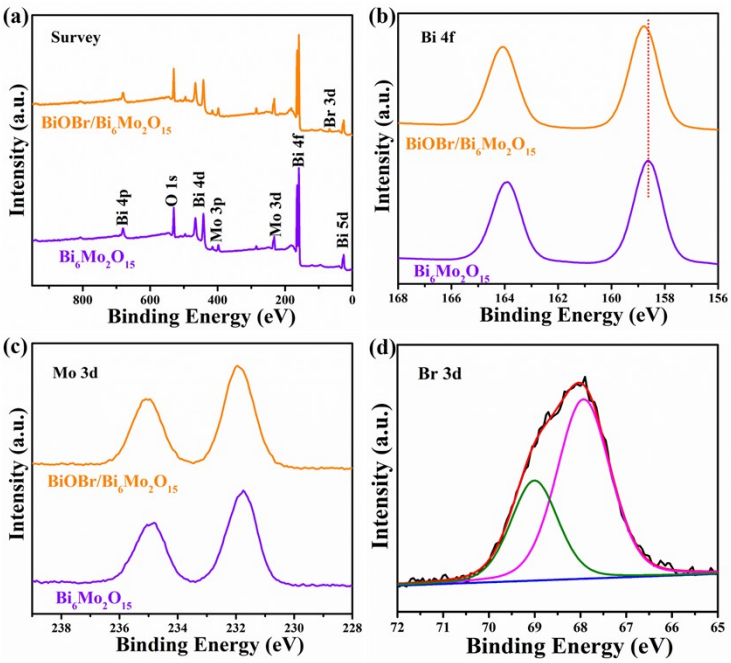

Fig. S5 XPS spectra of amples, full survey spectra (a) survey, Bi 4f (b), Mo 3d (c) and Br 3d (d).

XPS spectra of the $Bi_6Mo_2O_{15}$ and BiOBr/$Bi_6Mo_2O_{15}$ heterojunction were taken to reveal the chemical valence state of components. From Fig. S3a, the XPS survey spectrum of $Bi_6Mo_2O_{15}$ showed the signals of Bi, Mo and O elements, while the Bi, Mo, O and Br signals could be clearly observed in the BiOBr/$Bi_6Mo_2O_{15}$ survey spectrum. No other elements were discerned, suggesting the high purity of catalysts. As shown in Fig. S3b, two featured peaks with the binding energy of 158.61 and 163.93 eV were consistent with the Bi $4f_{7/2}$ and Bi $4f_{5/2}$ of Bi^{3+}.[1] However, A shift of 0.1-0.2 eV toward the higher Bi 4f binding energies could be observed in the BiOBr/Bi_4MoO_9 heterojunction, which might be due to the charge transfer caused by the strong interaction between BiOBr and $Bi_6Mo_2O_{15}$. As presented in Fig. S3c, two main signals for Mo $3d_{5/2}$ and Mo $3d_{3/2}$ centered at 231.76 and 234.93 eV originated from oxidized Mo^{6+}.[2] Additionally, the Br 3d spectrum of BiOBr/Bi_4MoO_9 (Fig. S3d) demonstrated the major peak at 67.92 and 69.02 eV, which could be assigned to the typical binding energy of Br^- ions.[3]

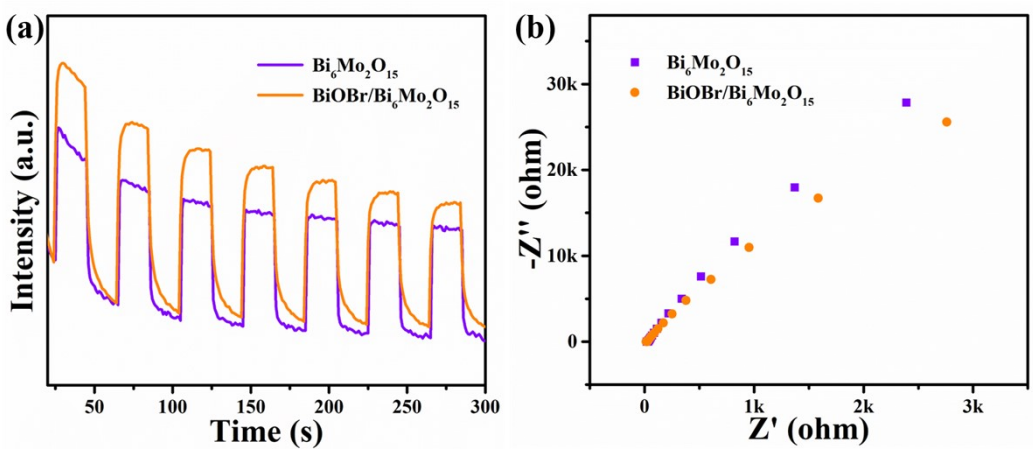

Fig. S6 (a) Plots of photocurrent density vs. irradiation time, and (b) EIS spectra of $Bi_6Mo_2O_{15}$ and BiOBr/$Bi_6Mo_2O_{15}$.

To illustrate the reasons for the enhanced photocatalytic activity of the

$BiOBr/Bi_6Mo_2O_{15}$ composite, the photocurrent-time measurement and EIS were exploited to characterize the $Bi_6Mo_2O_{15}$ and $BiOBr/Bi_6Mo_2O_{15}$ samples. As shown in Fig. S6a, the photocurrent density of $BiOBr/Bi_6Mo_2O_{15}$ composite was much greater than that of $Bi_6Mo_2O_{15}$, which indicated that more charge carriers in $BiOBr/Bi_6Mo_2O_{15}$. Fig. S6b describes the EIS Nyquist plots of $Bi_6Mo_2O_{15}$ and $BiOBr/Bi_6Mo_2O_{15}$. It could be seen that the diameter of the arc radius for the $BiOBr/Bi_6Mo_2O_{15}$ sample was smaller than $Bi_6Mo_2O_{15}$. These results showed that the formation of $BiOBr/Bi_6Mo_2O_{15}$ heterojunction inhibited the recombination of photogenerated carriers, which was conducive to the separation and transfer of photogenerated carriers in photocatalytic reaction.

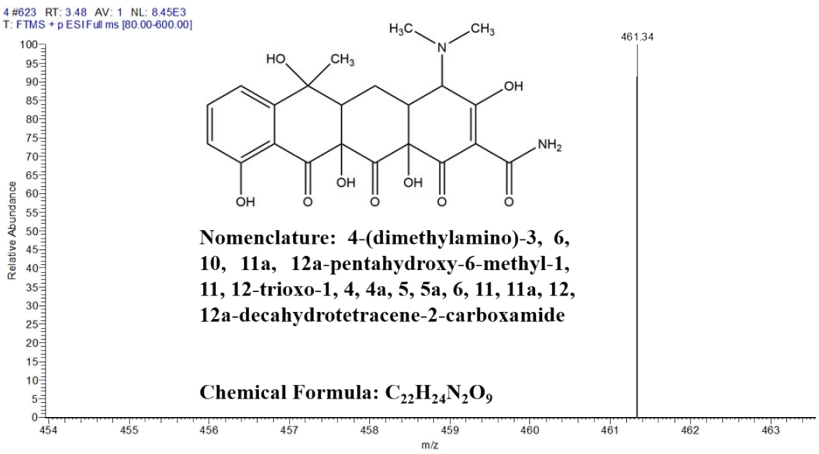

Fig. S7 The MS of TC (I) [m/z = 461] and the naming of compound.

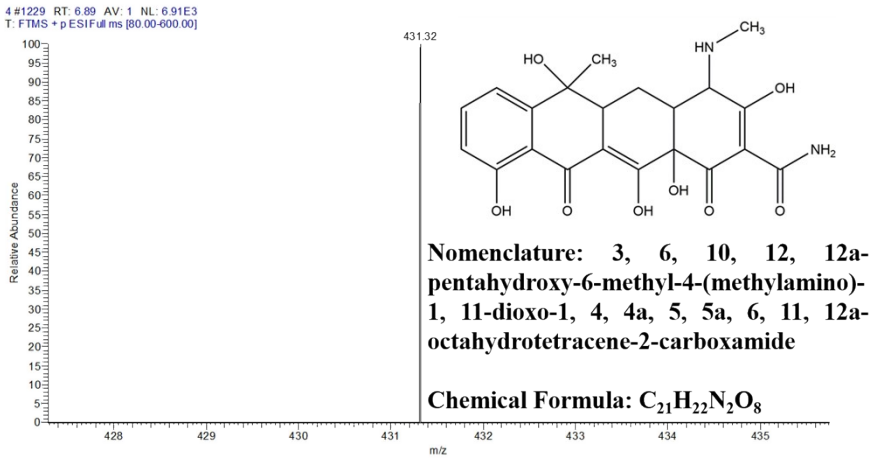

Fig. S8 The MS of TC (II) [m/z = 431] and the naming of compound.

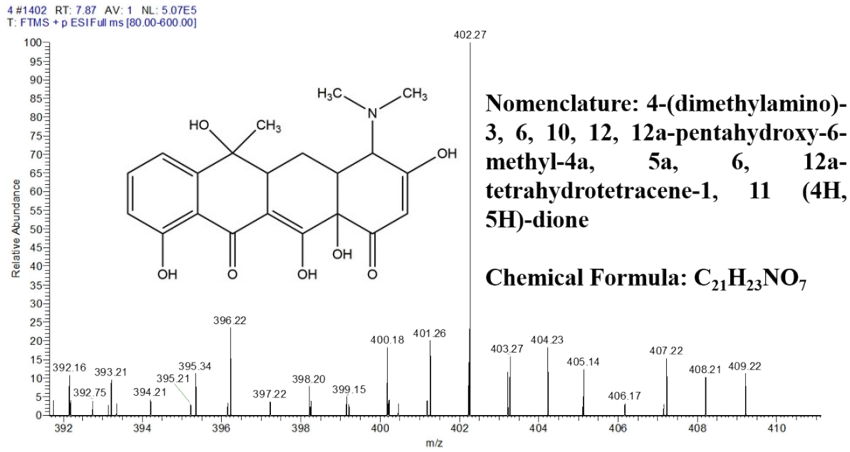

Fig. S9 The MS of TC (III) [m/z = 402] and the naming of compound.

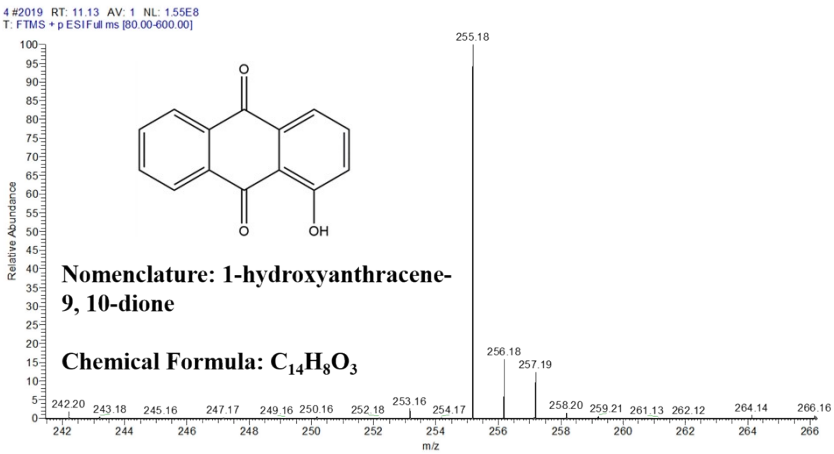

Fig. S10 The MS of TC (IV) [m/z = 255] and the naming of compound.

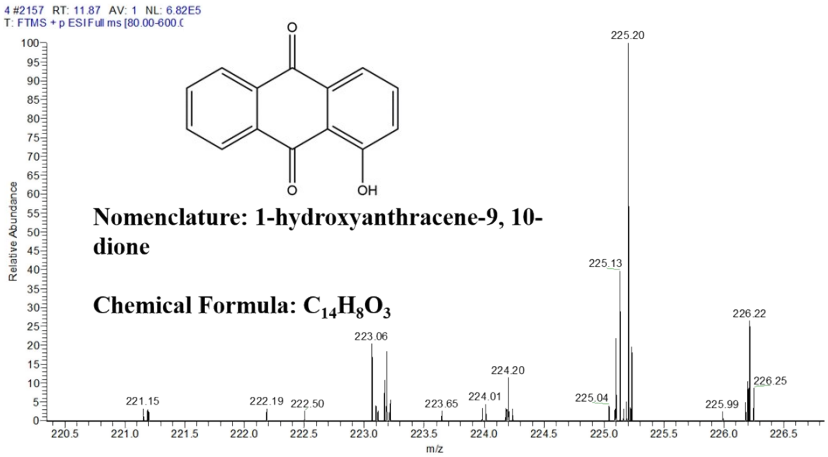

Fig. S11 The MS of TC (V) [m/z = 225] and the naming of compound.

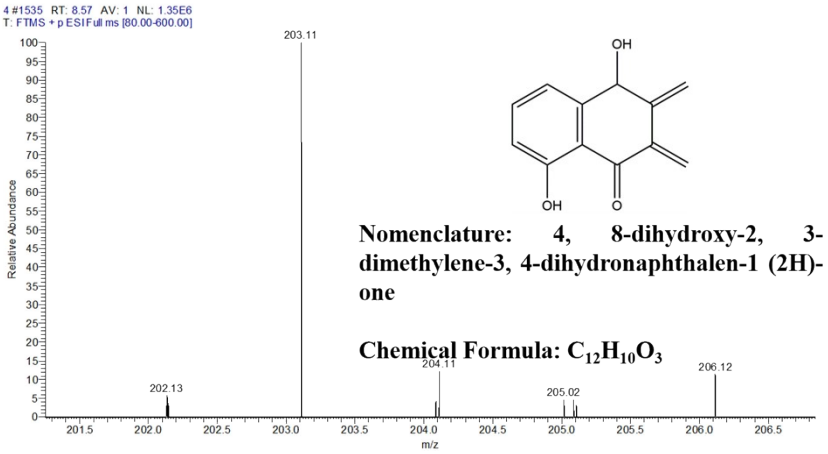

Fig. S12 The MS of TC (VI) [m/z = 203] and the naming of compound.

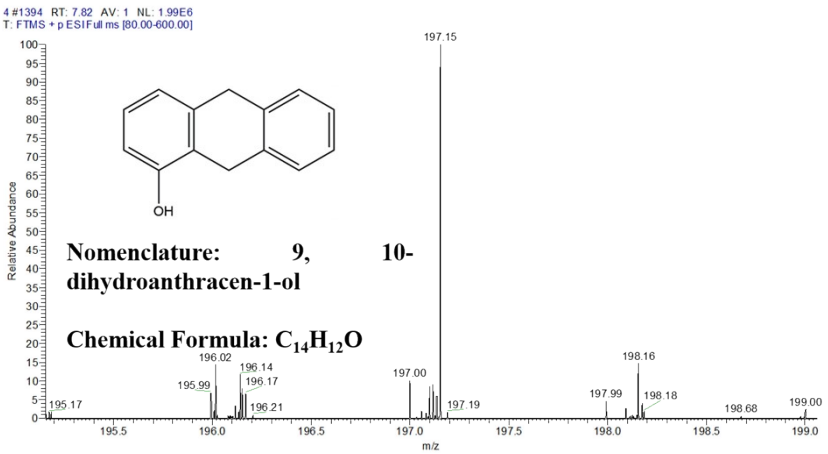

Fig. S13 The MS of TC (VII) [m/z = 197] and the naming of compound.

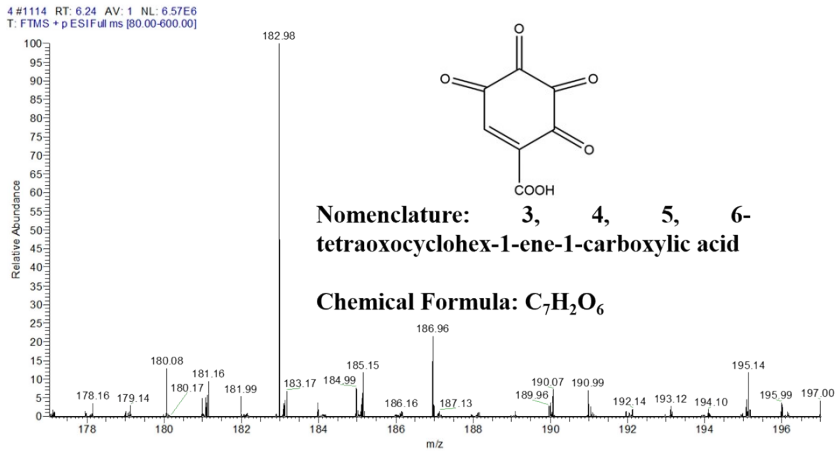

Fig. S14 The MS of TC (VIII) [m/z = 183] and the naming of compound.

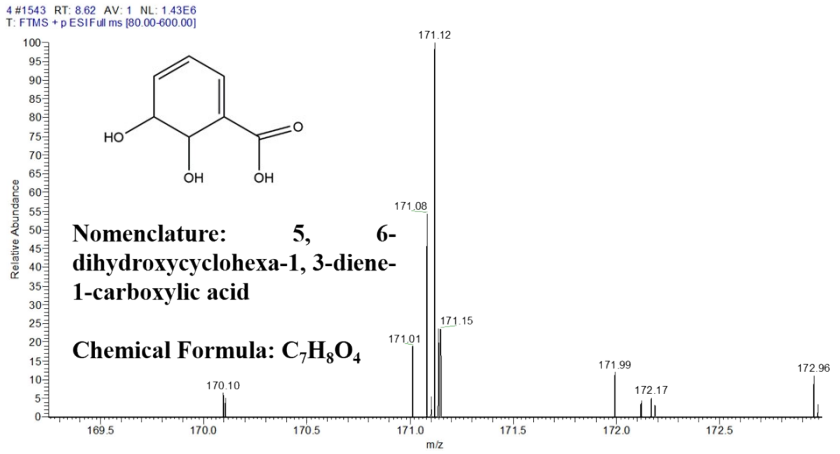

Fig. S15 The MS of TC (IX) [m/z = 171] and the naming of compound.

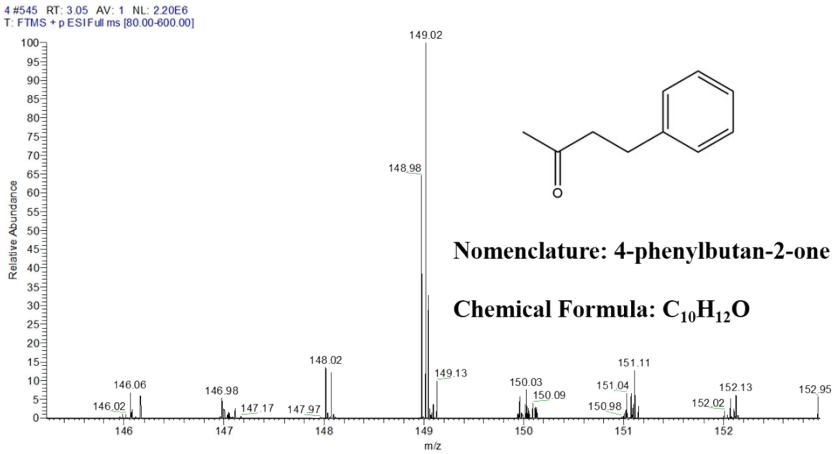

Fig. S16 The MS of TC (X) [m/z = 149] and the naming of compound.

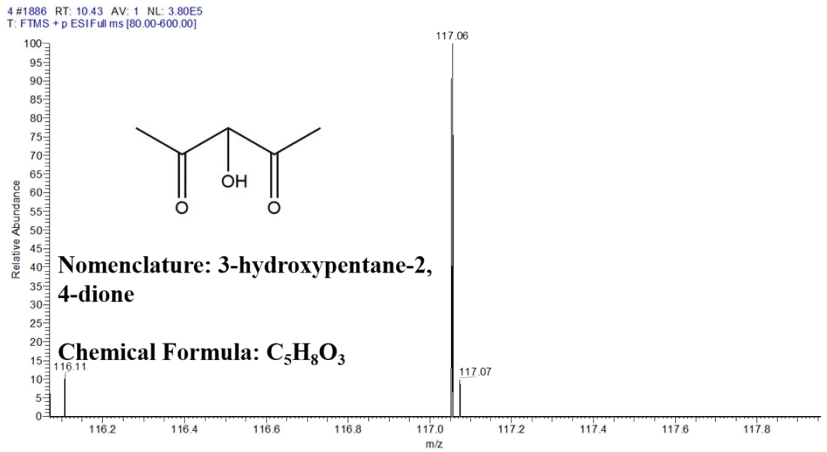

Fig. S17 The MS of TC (XI) [m/z = 117] and the naming of compound.

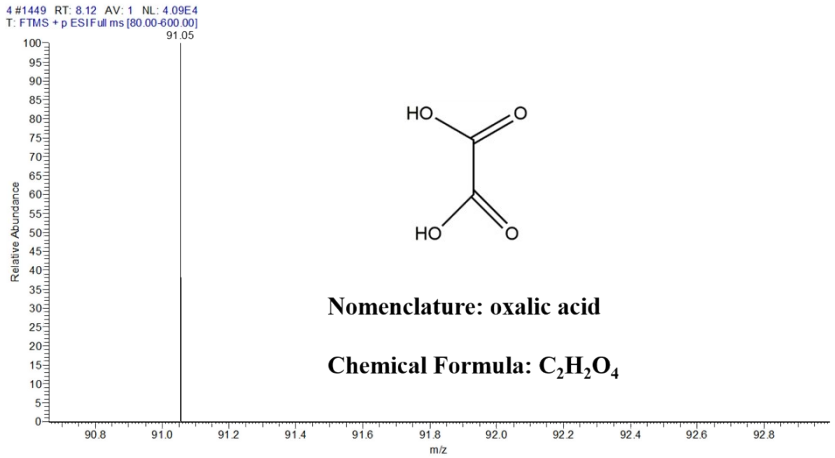

Fig. S18 The MS of TC (XII) [m/z = 91] and the naming of compound.

Table 1 Possible degradation intermediates identified by LC-MS.

Retention time (min)	m/z	Possible structure
3.48	461	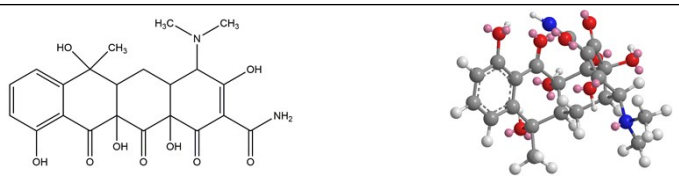
6.89	431	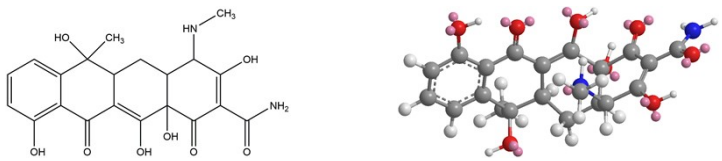

7.87	402	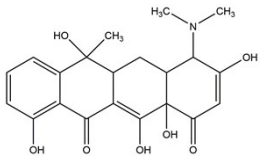	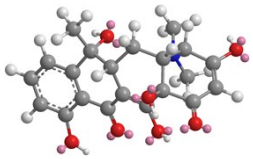
11.13	255	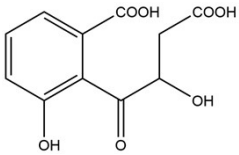	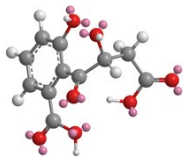
11.87	225	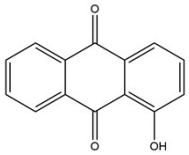	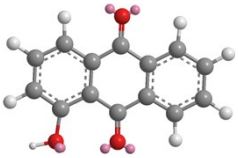
8.57	203	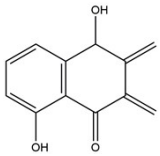	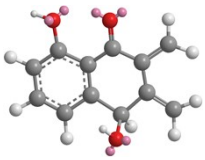
7.82	197	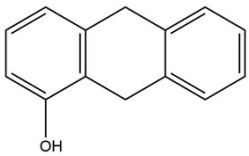	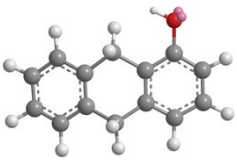
6.24	183	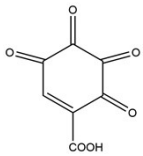	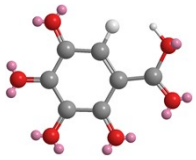
8.62	171	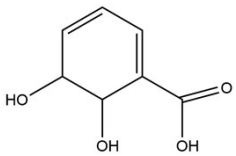	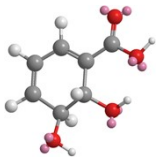
3.05	149	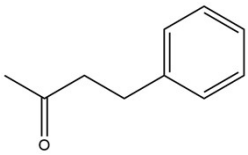	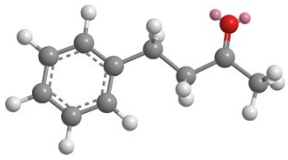
10.43	117	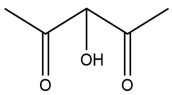	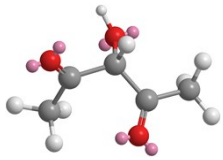
8.12	91	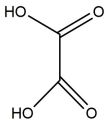	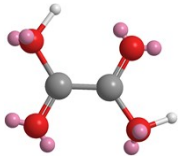

Notes and references

[1] J. Lv, K. Dai, J. Zhang, L. Geng, C. Liang, Q. Liu, G. Zhu and C. Chen, *Appl. Surf. Sci.*, 2015, **358**, 377-384.

[2] Y. Chen, G. Tian, Y. Shi, Y. Xiao and H. Fu, *Appl. Catal. B: Environ.*, 2015, **164**, 40-47.

[3] L. Ruan, J. Liu, Q. Zhou, J. Hu, G. Xu, X. Shu and Y. Wu, New J. Chem., 2014, **38**, 3022-3028.